Coulomb blockade regime of a single-wall carbon nanotube

A. A. Nersesyan[1,2] and A. M. Tsvelik[3]
[1]*The Abdus Salam International Centre for Theoretical Physics, Strada Costiera 11, 34100 Trieste, Italy*
[2]*The Andronikashvili Institute of Physics, Tamarashvili 6, 380077 Tbilisi, Georgia*
[3]*Department of Physics, Brookhaven National Laboratory, Upton, New York 11973-5000, USA*
(Received 14 May 2003; revised manuscript received 29 September 2003; published 30 December 2003)

We study a model of carbon nanotube with a half filled conduction band. At this filling the system is a Mott insulator. The Coulomb interaction is assumed to be unscreened. It is shown that this allows to develop the adiabatic approximation which leads to considerable simplifications in calculations of the excitation spectrum. We give a detailed analysis of the spectrum and the phase diagram at half filling, and discuss effects of small doping. In the latter case several phases develop strong superconducting fluctuations corresponding to various types of pairing.

DOI: 10.1103/PhysRevB.68.235419 PACS number(s): 71.10.Pm, 72.80.Sk

I. INTRODUCTION

Carbon nanotubes have attracted an enormous amount of attention and generated an immense level of theoretical and experimental activity. It has been rightly pointed out that single-wall carbon nanotubes (SWCN) represent ideal one-dimensional (1D) systems and one may expect to observe here exotic phenomena characteristic for strong correlations in one dimension. Most of the attention has been concentrated on a possibility of Tomonaga-Luttinger liquid. Though such liquid is certainly a very interesting object, it is just one of many wonders strong correlations can produce.

In this paper we concentrate on the physics of an armchair SWCN at half filling. The features which dominate this physics are the unscreened Coulomb interaction and Umklapp processes. The importance of the unscreened Coulomb interaction for nanotubes away from half filling was already noticed in the previous studies.[1,2] At half filling some additional factors come into play. It was realized in Ref. 3 that the long-range Coulomb interaction makes the operators responsible for the Umklapp scattering terms relevant. Consequently, the gaps for collective excitations generated by such operators are not exponentially small, as it would be away from half filling, but have power-law dependence on the Umklapp scattering matrix elements. Such enhancement of the gaps increases chances for their experimental observation. Unfortunately, in their further analysis the authors of Ref. 3 resorted to renormalization group (RG) equations, which for systems with many fields do not provide much insight into the properties at the strong-coupling fixed point. RG equations also do not take into account the drastic difference between velocities of the plasma modes and all other collective excitations. Instead of adding difficulties, however, the difference in velocities leads to considerable simplifications in actual calculations (see Ref. 4). In this paper we shall exploit this feature to our advantage and develop an approach based on the adiabatic approximation similar to the one used for the problem of electron-phonon interaction. As a result we will be able to provide a rather detailed information about the spectrum and the phase diagram of the system. As will be shown below, the interplay of the long-range Coulomb interaction and Umklapp processes at half filling gives rise to a phase diagram which includes several interesting strongly correlated states. The system has a hidden $Z_2\times Z_2\times Z_2$ symmetry and these phases are conveniently classified as different symmetry-breaking patterns of this group.

II. THE PROBLEM OF SINGLE-CHANNEL WIRE AT HALF FILLING

To warm up, let us first recall the problem of the unscreened Coulomb interaction for a single chain (or a single channel quantum wire) at half filling. The charge and spin sectors decouple; the Tomonaga-Luttinger liquid Hamiltonian for the charge sector should be supplemented by the Umklapp term which contains only the charge field Φ_c:

$$\mathcal{V}=Ua_0(R_\uparrow^+L_\uparrow R_\downarrow^+L_\downarrow+\text{H.c.})=\frac{U}{2\pi^2a_0}\cos[\sqrt{8\pi}\Phi_c], \quad (1)$$

where Ua_0 is the $2k_F=\pi$ Fourier component of the interaction. The full Hamiltonian density for the charge sector is $\mathcal{H}=\mathcal{H}_0+\mathcal{V}$, where

$$\mathcal{H}_0=\frac{1}{2}\left[(\hat{\pi}_c)^2+(\partial_x\Phi_c)\int dy V(x-y)(\partial_y\Phi_c)\right],$$

$$V(x)=v^2\delta(x)+\frac{e^2v}{\pi|x|}, \quad (2)$$

v being the Fermi velocity. This model is very close to the sine-Gordon one. The spectrum contains solitons and their bound states (breathers or excitons). To get their spectrum one can just expand the cosine around its minimum and obtain

$$\omega^2=(vq)^2\left[1+\frac{2e^2}{\pi v}\ln(1/qa_0)\right]+m_b^2, \quad (3)$$

where the breather gap is $m_b=(2/\pi)\sqrt{U\epsilon_F}$, $\epsilon_F=\pi v/a_0$. The breathers are effectively optical phonons of the one-dimensional Wigner crystal.[5] The soliton gap is larger; it was estimated in Ref. 4, a better estimate is

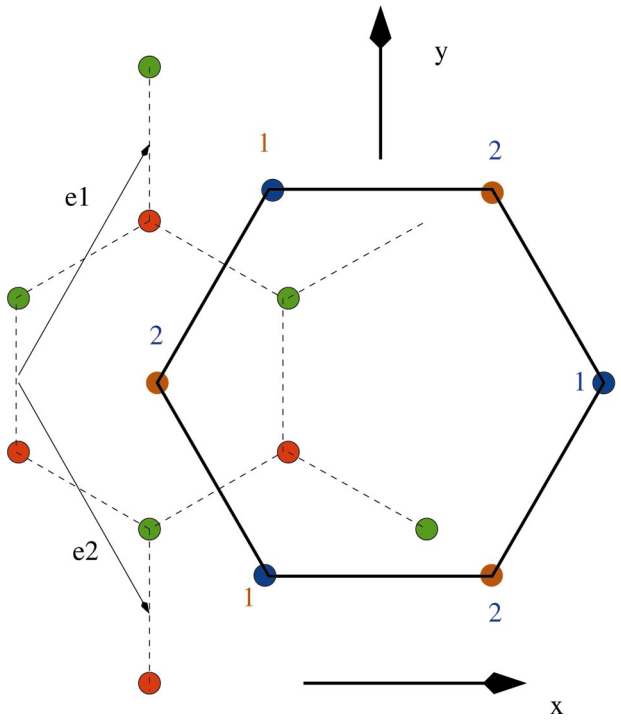

FIG. 1. (Color) The Bravais lattice cell (shown in dotted lines) including two inequivalent carbon ions (shown in red and green) and the Brillouin zone for graphite. $\mathbf{e}_1$ and $\mathbf{e}_2$ are basis vectors of the diatomic unit cell. The positions of the tips of two Dirac cones labeled by 1 and 2 are represented by blue and brown dots.

$$M_s=\frac{1}{\pi}[1+(2e^2/\pi v)\ln(v/M_s a_0)]\sqrt{U\epsilon_F}. \tag{4}$$

The spectrum in the spin sector is gapless, and the spin velocity is approximately v. Thus already for a simple one-chain problem, the long-distant Coulomb force brings three important new features: (i) strong upward renormalization of the charge velocity seen in Eq. (3), (ii) the presence of exciton modes in the charge sector, and (iii) power-law dependence of the mass scales M_s, m_b on the Umklapp matrix element U.

III. THE EXCITATION SPECTRUM OF NANOTUBE AT HALF FILLING

SWCN's are manufactured by wrapping two-dimensional graphite sheets into cylinders (compactification). The electronic spectrum of an infinite graphite sheet contains two Dirac cones with different chirality, centered at different points of the Brillouin zone (the blue dots on Fig. 1). Under compactification the spectrum is divided into subbands corresponding to different quantized values of the transverse momentum. In the so-called armchair nanotubes $k_y=0$ remains an eigenvalue and the spectrum in the lowest subband stays gapless; at half filling it is also doubly degenerate at low energies. This degeneracy is a vestige of the double-cone structure of the two-dimensional dispersion. We discuss the spectrum in some detail in Appendix A; more detailed information can be obtained from the book.[6]

In Appendix B we derive the bosonized form of the effective low-energy Hamiltonian. The total Hamiltonian density is

$$\mathcal{H}=\mathcal{H}_0[\Phi_c^{(+)}]+\frac{1}{2}\sum_a [(\hat{\pi}^{(a)})^2+v^2(\partial_x\Phi^{(a)})^2]+\mathcal{V}, \tag{5}$$

where $\mathcal{H}_0$ is given by Eq. (2); $\Phi_c^{(+)}$ is the symmetric charge mode. The label a takes three values, $a=(c,-),(s,+),(s,-)$, corresponding to the antisymmetric charge field and symmetric and antisymmetric spin fields, respectively (see Appendix A). The interaction density $\mathcal{V}$ contains Umklapp terms

$$\begin{aligned}\mathcal{V}=&-\frac{1}{2(\pi\alpha)^2}\cos(\sqrt{4\pi}\Phi_c^{(+)})[g_c\cos(\sqrt{4\pi}\Phi_c^{(-)})\\&+(g_3-g_1)\cos(\sqrt{4\pi}\Phi_s^{(+)})+g_3\cos(\sqrt{4\pi}\Theta_s^{(-)})\\&-g_1\cos(\sqrt{4\pi}\Phi_s^{(-)})]+\cdots,\end{aligned} \tag{6}$$

where the dots stand for all other terms that do not involve $\Phi_c^{(+)}$ and stay marginal even in the presence of the unscreened Coulomb interaction. The couplings g_c, g_1, and g_3 are determined by the lattice Hamiltonian. In Appendix B we estimate them for realistic carbon nanotubes, where, as it turns out, $g_c=g_1$ and, hence, there are only two independent coupling constants. The unscreened Coulomb interaction strongly reduces the scaling dimension of the operator $\cos(\sqrt{4\pi}\Phi_c^{(+)})$ in the long-wavelength limit, making it smaller than 1. Thus the Umklapp terms (6) become strongly relevant, with the scaling dimension almost equal to 1. This circumstance dramatically increases the values of the gaps.

One may well expect that the double degeneracy of the electron band in carbon nanotubes makes the problem similar to the problem of two interacting chains (the ''ladder'' problem) much discussed in literature. This is indeed the case. To put the problem in a broader context, let us discuss two extreme types of ladders: (i) the ones where two chains are placed far apart such that there is no direct tunneling between them, and (ii) those in which the interchain tunneling is stronger than all the interactions. Hamiltonians (5) and (6) are formally equivalent to the first case describing two well separated chains. As a matter of fact, the Hamiltonian for case (ii) is not very different. The calculations done in Ref. 7 for the ladder with strong interchain tunneling yields the same Hamiltonian as Eq. (6), but with $\Phi_{c,-}$ field being substituted by its dual counterpart $\Theta_{c,-}$:

$$\mathcal{V}_B=\mathcal{V}_A[\Phi_{c,-}\to\Theta_{c,-}]. \tag{7}$$

Therefore one expects that the two models have the same excitation spectrum though the response functions are different due to the different field identification.

Hamiltonian (6) is not very convenient to analyze in its bosonic form since the effective potential contains mutually nonlocal and noncommuting fields, $\Phi_{s,-}$ and $\Theta_{s,-}$. The physics becomes significantly more transparent when one uses the refermionization procedure.[8,9] Fermionizing all the fields except of $\Phi_c^{(+)}$, we obtain

$$\mathcal{H}=\mathcal{H}_0[\Phi_c^{(+)}]+iv(-R_f^\dagger\partial_x R_f+L_f^\dagger\partial_x L_f)$$
$$+\frac{iv}{2}\sum_{a=0}^{3}(-\chi_R^a\partial_x\chi_R^a+\chi_L^a\partial_x\chi_L^a)-\frac{i}{\pi\alpha}\cos(\sqrt{4\pi}\Phi_c^{(+)})$$
$$\times\left[g_c(R_f^\dagger L_f-\text{H.c.})+2g_t\sum_{a=1}^{3}\chi_R^a\chi_L^a+2g_s\chi_R^0\chi_L^0\right],$$
$$g_c=g_1,\quad g_t=(g_3-g_1),\quad g_s=-g_1-g_3, \tag{8}$$

where χ_R,χ_L are Majorana (real) fermions and R_f,L_f are Dirac fermions emerging from the fermionization of the operator $\cos(\sqrt{4\pi}\Phi_{c,-})$ or, in the second case, $\cos(\sqrt{4\pi}\Theta_{c,-})$. Note that Eq. (8) is manifestly SU(2) symmetric. The triplet of Majorana fermions ($a=1,2,3$) transforms according to the spin $S=1$ representation of the SU(2) group, whereas the fermion labeled by $a=0$ is a singlet under the SU(2).

Following Ref. 10, we shall handle Hamiltonian (8) using the adiabatic approximation, whose validity is guaranteed by the fact that the velocity in the symmetric charge sector is strongly enhanced by the long-distant Coulomb interaction with respect to the bare Fermi velocity. The results have certain similarity with the SU(4) theory proposed in Ref. 11, but also contain important differences, which we shall discuss.

Thus, from the $\Phi_c^{(+)}$-mode point of view, the other degrees of freedom are static. Integrating over this mode, one obtains an effective potential for the fermions in the form of the ground-state energy of the sine-Gordon model. According to Ref. 12 the energy density is proportional to the square of the breather mass μ_b of such sine-Gordon model and in the regime of small sine-Gordon coupling constant β^2 is equal to

$$E\approx-\frac{\mu_b^2}{4\pi v_c}\approx-v/(\pi\alpha v_c)\left[ig_c(R_f^\dagger L_f-\text{H.c.})\right.$$
$$\left.+2ig_t\sum_{a=1}^{3}\chi_R^a\chi_L^a+2ig_s\chi_R^0\chi_L^0\right], \tag{9}$$

where $v_c\approx v_F[1+(2e^2/\pi v_F)\ln(\epsilon_F/M)]^{1/2}$ and $v\approx v_F$. So as we see, the integration over the fast mode gives rise to the mass terms for all of the fermions. The fermionic modes acquire gaps

$$M_{c,-}=\frac{vg_c}{\pi\alpha v_c},\quad M_{s,t}=\frac{vg_t}{\pi\alpha v_c},\quad M_{s,s}=\frac{vg_s}{\pi\alpha v_c}. \tag{10}$$

They correspond to neutral excitations with the quantum numbers given in the Table I that follows; see also Fig. 2. As far as the fast modes are concerned, one has to treat differently the ones with and without electric charge. The neutral modes do not involve solitons of field $\Phi_c^{(+)}$. One can get a good estimate of their spectrum replacing the term in the square brackets in expression for the Hamiltonian (8) by a constant and expanding around the minimum of the cosine potential. As a result one gets the same spectrum as for the single chain (3) with

TABLE I.

Mass	Q	S	V
$M_{s,t}$ triplet	0	1	0
$M_{s,s}$ singlet	0	0	0
$M_{c,-}$ vortex	0	0	±2
m_b breathers	0	0	0
M_e electron	±1	1/2	±1

$$m_b^2=\pi(M_{c,-}^2+3M_{s,t}^2+M_{s,s}^2)\ln(v/\alpha),$$

where with the logarithmic accuracy M is either $M_{c,-}$ or M_S. Thus

$$m_b/M\sim[\ln(v/\alpha M)]^{1/2}\gg1,$$

which further supports the adiabatic approximation. However, as we have already mentioned, its validity is already assured by the difference in the velocities. Apart from the breather modes there are massive modes corresponding to half-period solitons in $\Phi_c^{(+)}$ with zero modes of the fermions bound to them. These excitations have the largest gap (we call it M_e) and carry quantum numbers of electron.

The results for the spectrum are summarized in Table I; see also Fig. 2. Excitations are characterized by quantum numbers associated with the full continuous symmetry group of the effective model (8). These are the total charge Q measured in units of the electron charge e, total spin S, and ''vorticity'' V. Let us comment on the latter. While the global U(1) phase invariance and the spin SU(2) symmetry, leading to conservation of the total charge and spin,

$$Q=\frac{2}{\sqrt{\pi}}\int_{-\infty}^{\infty}\partial_x\Phi_c^{(+)}(x),\quad S^z=\frac{1}{\sqrt{\pi}}\int_{-\infty}^{\infty}\partial_x\Phi_s^{(+)}(x), \tag{11}$$

are exact symmetries of the original, microscopic Hamiltonian, an extra (''flavor'') U(1) symmetry generated by global phase transformations of the f spinor (R_f,L_f) (or equivalently, by uniform translations of the dual field $\Theta_c^{(-)}$), emerges in the low-energy limit only. This symmetry leads to conservation of the flavor charge

$$V=\frac{2}{\sqrt{\pi}}\int_{-\infty}^{\infty}\partial_x\Phi_c^{(-)}(x), \tag{12}$$

which, together with conservation of Q, implies independent conservation of the particle numbers at each Dirac point, $Q_{1,2}=(Q\pm V)/2$.

The nomenclature vorticity we have chosen follows from the microscopic origin of the flavor density. Indeed, consider a lattice operator describing a current flowing around the elementary plaquette of sublattice a or b:

$$j_{\text{plaq},\nu}(\mathbf{r})=i[\psi_\nu^\dagger(\mathbf{r})\psi_\nu(\mathbf{r}-\mathbf{e}_2)+\psi_\nu^\dagger(\mathbf{r}-\mathbf{e}_2)\psi_\nu(\mathbf{r}+\mathbf{e}_1)$$
$$+\psi_\nu^\dagger(\mathbf{r}+\mathbf{e}_1)\psi_\nu(\mathbf{r})-\text{H.c.}]$$
$$\nu=a,b. \tag{13}$$

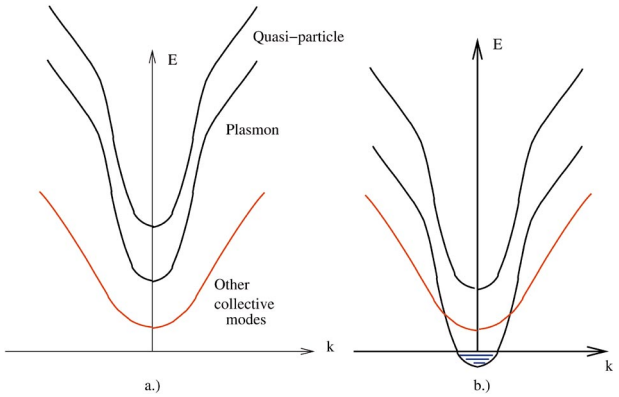

FIG. 2. (Color) A schematic picture of the excitation spectrum: (a) at half filling and (b) at small doping.

From this construction it follows that the state with a nonzero $\langle j_{\text{plaq, a(b)}}\rangle$ would represent an orbital antiferromagnet, or a staggered flux phase, realized on the sublattice a (b), as shown in Fig. 3. Projecting Eq. (13) onto the $k_y=0$ subband and passing to the continuum limit, one makes sure that the sum $\mathbf{j}_{\text{plaq},a}+\mathbf{j}_{\text{plaq},b}$ does transform to the flavor charge density

$$\rho_f=\sum_\sigma [:R^\dagger_{1\sigma}R_{1\sigma}:-:R^\dagger_{2\sigma}R_{2\sigma}:+(R\to L)]\sim\partial_x\Phi^{(-)}_{\text{c}}.$$

Previous attempts to study the problem of two coupled channels have mostly relied on the assumption of equal velocities with the subsequent use of RG analysis. The approach was pioneered by Lin *et al.*[11] who argued that at strong coupling the spectrum of the two-chain problem at half filling acquires a higher symmetry, such as SO(6) or even SO(8). In fact, Gell-Mann-Low equations alone are insufficient to extract information about strong-coupling regime (they have to be supplemented by Callan-Symanzik equations for the physical observables) and therefore cannot provide a legitimate ground for such conclusions. Our approach is based on a different assumption; here the long-range Coulomb interaction legitimates a clear separation of scales between single-particle excitations and collective modes. This significantly simplifies the calculations providing one with the well-controlled approximation. It is instructive to compare the results with those conjectured in Ref. 11. Though the structure of the multiplets is the same as in the $\text{SU}(4)\sim\text{SO}(6)$ theory, there are important differences in the spectrum. Two quasiparticle multiplets (particles and antiparticles) are fourfold degenerate, as in the SU(4) theory, but the sixfold degenerate multiplet of the SU(4) is split into a doublet with the mass $M_{\text{c},-}$, a magnetic triplet with the mass $M_{\text{S},t}$, and a singlet mode with the mass $M_{\text{S},s}$. The ratios of the quasiparticle mass to the masses of the neutral modes are vastly different from the SU(4) Gross-Neveu model ratio $M_{\text{S}}/M_e=\sqrt{2}$. They depend on the Coulomb interaction and the quasiparticle gap is much larger than the spin and the parity collective-mode gaps. The gaps of the collective modes are not equal. In nanotubes where there are only two independent coupling constants we expect that

$$2M_{\text{c}}+M_t+M_s=0 \tag{14}$$

(recall that since we deal with Majorana fermions, the masses may be negative, the spectral gaps being their absolute values).

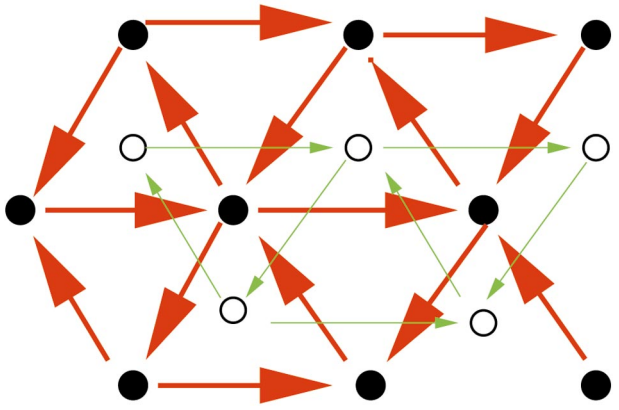

FIG. 3. (Color) A staggered flux (orbital antiferromagnet) state corresponding to a nonzero value of vorticity V. The arrows indicate local currents flowing across the links of the a (red) and b (green) sublattices.

IV. THE ORDER PARAMETERS OF DIFFERENT PHASES

From now on we shall concentrate on the model describing carbon nanotubes. Different phases, shown in Fig. 3, correspond to different ground-state phase lockings and are determined by the signs of the fermionic masses,[8] Eqs. (10). These sign changes are not reflected in the thermodynamics which is sensitive only to absolute values of the masses. The difference in the correlation functions may, however, be quite dramatic.

We use the following conventions:[8]

$$\cos(\sqrt{\pi}\Phi^{(+)}_s)=\sigma_1\sigma_2,\quad \sin(\sqrt{\pi}\Phi^{(+)}_s)=\mu_1\mu_2,$$
$$\cos(\sqrt{\pi}\Theta^{(+)}_s)=\mu_1\sigma_2,\quad \sin(\sqrt{\pi}\Theta^{(+)}_s)=\sigma_1\mu_2, \tag{15}$$
$$\cos(\sqrt{\pi}\Phi^{(-)}_s)=\sigma_0\sigma_3,\quad \sin(\sqrt{\pi}\Phi^{(-)}_s)=\mu_0\mu_3,$$
$$\cos(\sqrt{\pi}\Theta^{(-)}_s)=\mu_0\sigma_3,\quad \sin(\sqrt{\pi}\Theta^{(-)}_s)=\sigma_0\mu_3 \tag{16}$$

where $\{\sigma_i\}$ and $\{\mu_i\}(i=1,2,3,0)$ are order and disorder parameters of the 2D Ising models associated with the singlet $(i=1,2,3)$ and triplet $(i=0)$ Majorana fermions. A particular Ising model is ordered $(\langle\sigma\rangle\neq0)$ or disordered $(\langle\mu\rangle\neq0)$ depending on the sign of the corresponding Majorana mass, $M<0$ or $M>0$. In order to understand the structure and properties of the correlation functions, one has to recall that in the ordered phase of the Ising model, where $\langle\sigma\rangle\neq0$, the correlation function $\langle\langle\mu(\omega,q)\mu(-\omega,-q)\rangle\rangle$ contains a coherent peak, while the correlation function of the σ's does not.

There are six possible phases, two of them being Haldane spin liquids. Such liquids are characterized by the presence of a coherent triplet magnetic excitation (magnon) in the two-point correlation function of the staggered magnetiza-

TABLE II.

Phase			
A	$\langle\cos(\sqrt{\pi}\Phi_c^{(-)})\rangle\neq 0$	$\langle\sigma_a\rangle\neq 0$	$\langle\sigma_0\rangle\neq 0$
B	$\langle\cos(\sqrt{\pi}\Phi_c^{(-)})\rangle\neq 0$	$\langle\mu_a\rangle\neq 0$	$\langle\sigma_0\rangle\neq 0$
C	$\langle\sin(\sqrt{\pi}\Phi_c^{(-)})\rangle\neq 0$	$\langle\mu_a\rangle\neq 0$	$\langle\sigma_0\rangle\neq 0$
D	$\langle\sin(\sqrt{\pi}\Phi_c^{(-)})\rangle\neq 0$	$\langle\mu_a\rangle\neq 0$	$\langle\mu_0\rangle\neq 0$
E	$\langle\sin(\sqrt{\pi}\Phi_c^{(-)})\rangle\neq 0$	$\langle\sigma_a\rangle\neq 0$	$\langle\mu_0\rangle\neq 0$
F	$\langle\cos(\sqrt{\pi}\Phi_c^{(-)})\rangle\neq 0$	$\langle\sigma_a\rangle\neq 0$	$\langle\mu_0\rangle\neq 0$

tions. In non-Haldane disordered phases, the spectrum of triplet excitations is incoherent; however spin-singlet modes may be coherent. Table II and Fig. 3 show which operators acquire nonzero expectation values in the corresponding ground states. It will be assumed that in all phases the symmetric charge field is locked at $\Phi_c^{(+)}=0$, so that $\langle\cos\sqrt{\pi}\Phi_c^{(+)}\rangle\neq 0$, $\langle\sin\sqrt{\pi}\Phi_c^{(+)}\rangle=0$.

Below we give a brief characterization of each phase; for more details see the subsequent discussion.

(1) Phase *A*: $g_1>|g_3|$. This phase has a long-range bond density wave (BDW) order at $T=0$ (see Fig. 4 below).

(2) Phase *B*: $0<g_1<g_3$. This is a Haldane spin-liquid phase whose excitation spectrum contains a coherent triplet magnon with the mass $M_{S,t}$, associated with the correlation function of the site-diagonal spin operator $\mathbf{S}^{(-)}$; see Eq. (24). Under doping it develops a power-law response of the pairing susceptibility of type described further in the text. The corresponding superconducting order parameter transforms nontrivially under the lattice point group.

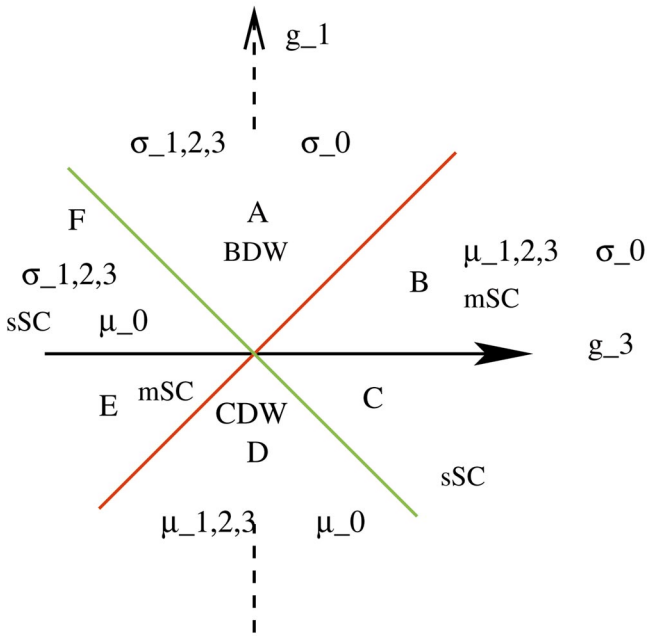

FIG. 4. (Color) The phase diagram. For each quadrant it is indicated which Ising-models order and disorder parameters have nonzero ground-state expectation values. The phases are separated by critical lines on which one of the particle masses vanishes. The green and red lines are Z_2 and $SU_2(2)$ critical lines respectively. The $g_1=0$ axis corresponds to the $U(1)$ critical line. Phases *A* and *D* have density wave order. Under doping phases *B*, *E*, and *C*, *F* develop a power-law response to superconducting paring.

(3) Non-Haldane phase *C*: $-g_3<g_1<0$. The magnetic singlet mode with mass $M_{S,s}$ becomes coherent in this phase. As a result a coherent peak appears in the correlation function of the charge-density wave order parameter Δ_{CDW}, Eq. (18). Under doping this phase develops superconducting correlations in the *s* channel.

(4) Phase *D*: $g_1<-|g_3|$. There is a charge-density wave (CDW) long-range order in the ground state of this phase. Phases CDW and BDW are mutually dual.

(5) Phase *E*: $g_3<g_1<0$. This is another Haldane phase dual to phase *B*. Phase *E* has a coherent magnon in the site-off-diagonal spin density $\mathbf{\Sigma}^{(-)}$, Eq. (25). Under doping it develops superconducting correlations of the same type as phase *B*.

(6) Phase *F*: $0<g_1<-g_3$. This phase is dual to phase *C* and has a coherent spin-singlet mode displayed by the BDW order-parameter correlation function. Under doping it develops superconducting correlations in the *s* channel.

A. Order parameters, possible orderings, and dominant correlations

CDW. Already for geometrical reasons (the lattice is bipartite) one may expect that the system at half filling can develop a commensurate charge-density wave. Introducing locally averaged electron densities for *a* and *b* sublattices,

$$\overline{\rho}_\nu(\mathbf{r})=\tfrac{1}{3}[\psi_\nu^\dagger\psi_\nu(\mathbf{r})+\psi_\nu^\dagger\psi_\nu(\mathbf{r}+\mathbf{e}_1)+\psi_\nu^\dagger\psi_\nu(\mathbf{r}-\mathbf{e}_2)],$$

$$\nu=a,b, \tag{17}$$

we define the CDW order parameter (OP) as follows:

$$\begin{aligned}\Delta_{CDW}(\mathbf{r})&=\overline{\rho}_a(\mathbf{r})-\overline{\rho}_b(\mathbf{r})\\ &\sim\sum_\sigma (R_{1\sigma}^\dagger L_{1\sigma}-R_{2\sigma}^\dagger L_{2\sigma})+\text{H.c.}\\ &\sim\sin(\sqrt{\pi}\Phi_c^{(+)})\cos(\sqrt{\pi}\Phi_c^{(-)})\sigma_1\sigma_2\sigma_3\sigma_0\\ &\quad-\cos(\sqrt{\pi}\Phi_c^{(+)})\sin(\sqrt{\pi}\Phi_c^{(-)})\mu_1\mu_2\mu_3\mu_0.\end{aligned} \tag{18}$$

This OP has a nonzero average value in phase *D*. In phase *C* where $\langle\sin(\sqrt{\pi}\Phi_c^{(-)})\rangle\neq 0$ and $\langle\mu_a\rangle\neq 0$ $(a=1,2,3)$, the most singular part of the CDW order parameter is proportional to μ_0. Since we are in the phase with $\langle\sigma_0\rangle\neq 0$, operator μ_0 has a nonzero matrix element between the ground state and a state with one Majorana fermion. Therefore, the correlation function of CDW OP's contains a coherent peak corresponding to an emission of the singlet magnetic mode with the mass $M_{S,s}$.

BDW. The bond density wave order parameter is similar to the CDW one, but is off diagonal in the site indices,

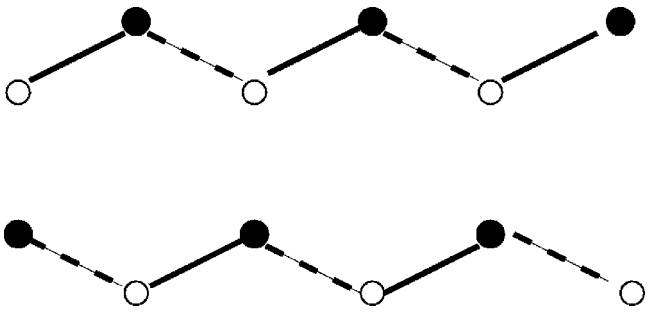

FIG. 5. The dimerization in BDW phase.

$$\Delta_{BDW}(\mathbf{r}) = \psi_a^\dagger(\mathbf{r})[\psi_b(\mathbf{r}+\mathbf{e}_1) - \psi_b(\mathbf{r}-\mathbf{e}_2)] - [\psi_a^\dagger(\mathbf{r}+\mathbf{e}_1) - \psi_a^\dagger(\mathbf{r}-\mathbf{e}_2)]\psi_b(\mathbf{r}) + \text{H.c.}$$

$$\sim i\sum_\sigma (R_{1\sigma}^\dagger L_{1\sigma} - R_{2\sigma}^\dagger L_{2\sigma}) + \text{H.c.}$$

$$\sim \sin(\sqrt{\pi}\Phi_c^{(+)})\sin(\sqrt{\pi}\Phi_c^{(-)})\mu_1\mu_2\mu_3\mu_0 + \cos(\sqrt{\pi}\Phi_c^{(+)})\cos(\sqrt{\pi}\Phi_c^{(-)})\sigma_1\sigma_2\sigma_3\sigma_0. \quad (19)$$

This phase is dual to the CDW one. The BDW order parameter condenses in phase *A*. The dimerization ordering pattern in this phase is shown in Fig. 4. In the disordered phase *F* (which is dual to phase *C*), the spectral weight of the OP Δ_{BDW} contains a coherent magnetic singlet mode with the mass $M_{S,s}$.

Note that the CDW and BDW OP's do not contain any (Fig. 5) oscillatory pieces. These show up in the density distributions that are not uniform across a sublattice but otherwise are consistent with the uniaxial symmetry of the nanotube,

$$\tilde{\rho}_\nu(\mathbf{r}) = \tfrac{1}{2}[\psi_\nu^\dagger\psi_\nu(\mathbf{r}+\mathbf{e}_1) + \psi_\nu^\dagger\psi_\nu(\mathbf{r}-\mathbf{e}_2) - \psi_\nu^\dagger\psi_\nu(\mathbf{r})],$$

$$\nu = a,b.$$

Two incommensurate CDW OP's can then be constructed as follows:

$$\Delta_{mCDW}^{(+)}(\mathbf{r}) = \tilde{\rho}_a(\mathbf{r}) + \tilde{\rho}_b(\mathbf{r})$$

$$\sim e^{-2iQx}\sum_\sigma (L_{1\sigma}^\dagger R_{2\sigma} - R_{1\sigma}^\dagger L_{2\sigma}) + \text{H.c.}$$

$$\sim i\kappa_{1\uparrow}\kappa_{2\uparrow}e^{-2iQx}e^{i\sqrt{\pi}\Theta_c^{(-)}} \times[\sin(\sqrt{\pi}\Phi_c^{(+)})\mu_1\mu_2\mu_3\sigma_0 + i\cos(\sqrt{\pi}\Phi^{(+)})\sigma_1\sigma_2\sigma_3\mu_0] + \text{H.c.}, \quad (20)$$

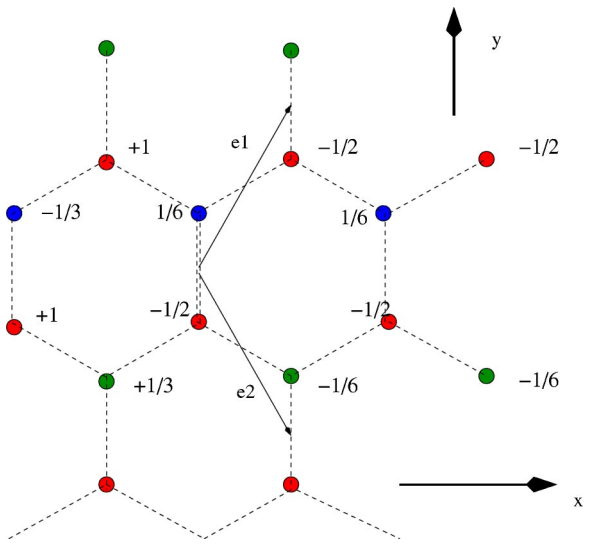

FIG. 6. (Color) The charge distribution for the mCDW order.

$$\Delta_{mCDW}^{(-)}(\mathbf{r}) = \tilde{\rho}_a(\mathbf{r}) - \tilde{\rho}_b(\mathbf{r})$$

$$\sim e^{-2iQx}\sum_\sigma (R_{1\sigma}^\dagger R_{2\sigma} - L_{1\sigma}^\dagger L_{2\sigma}) + \text{H.c.}$$

$$\sim \kappa_{1\uparrow}\kappa_{2\uparrow}e^{-2iQx}[R_f^\dagger\chi_R^{(0)} + L_f^\dagger\chi_L^{(0)}] + \text{H.c.}, \quad (21)$$

where κ's are Klein factors. Since the dual antisymmetric charge field $\Theta_c^{(-)}$ is strongly disordered ($\langle e^{i\sqrt{\pi}\Theta_c^{(-)}}\rangle = 0$), the OP $\Delta_{mCDW}^{(+)}$ has zero expectation value in all sectors of the phase diagram. In phase *F*, where $\langle\sigma_a\rangle \neq 0 (a = 1,2,3)$, $\langle\mu_0\rangle \neq 0$, the correlation function of the mCDW$^+$ OP displays a coherent peak corresponding to emission of a vortex particle with the mass $M_{c,-}$.

The charge distribution corresponding to the OP $\Delta_{mCDW}^{(-)}$ is depicted in Fig. 6. This kind of order can be induced by applying a modulated potential of sufficient strength that couples to Δ_{mCDW}^{-}. The potential must be strong enough to overcome the energy gaps of the corresponding excitation branches and to drive the system into a state with an induced order of the mCDW$^-$ type.

Magnetization. The total magnetization is given by

$$\mathbf{S}_+ = \tfrac{1}{2}\psi_a^\dagger\boldsymbol{\sigma}\psi_a + \tfrac{1}{2}\psi_b^\dagger\boldsymbol{\sigma}\psi_b = \mathbf{I}_R + \mathbf{I}_L + \tfrac{1}{2}\{e^{2iQx}[(R_2^+\boldsymbol{\sigma}L_1) - (L_2^+\boldsymbol{\sigma}R_1)] + \text{H.c.}\}.$$

Its smooth part is equal to the sum of the chiral currents of the Majorana triplet,

$$I_{R(L)}^a = J_{1,R(L)}^a + J_{2,R(L)}^a = -\frac{i}{2}\epsilon^{abc}\chi_{R(L)}^b\chi_{R(L)}^c.$$

The oscillating part of the spin density is (Klein factors omitted)

$$\mathbf{S}_{2Q}^{(+)} \sim e^{i\sqrt{\pi}\Theta_c^{(-)}}[-\sin(\sqrt{\pi}\Phi_c^{(+)})\mu_0\mathbf{N} + i\cos(\sqrt{\pi}\Phi_c^{(+)})\sigma_0\tilde{\mathbf{N}}]. \quad (22)$$

Here $\tilde{\mathbf{N}}=(\mu_1\sigma_2\sigma_3,\sigma_1\mu_2\sigma_3,\sigma_1\sigma_2\mu_3)$ and $\mathbf{N}=(\sigma_1\mu_2\sigma_3,\mu_1\sigma_2\mu_3,\mu_1\mu_2\sigma_3)$. This OP is never coherent.

On the other hand, to define the *staggered magnetization* $\mathbf{S}^{(-)}(\mathbf{r})$ associated with the bipartite lattice, we need to introduce locally averaged spin densities for the two sublattices [cf. Eq. (17)]:

$$\overline{\mathbf{s}}_\nu(\mathbf{r})=\tfrac{1}{6}[\psi_\nu^\dagger\boldsymbol{\sigma}\psi_\nu(\mathbf{r})+\psi_\nu^\dagger\boldsymbol{\sigma}\psi_\nu(\mathbf{r}+\mathbf{e}_1)+\psi_\nu^\dagger\boldsymbol{\sigma}\psi_\nu(\mathbf{r}-\mathbf{e}_2)],$$

$$\nu=a,b. \tag{23}$$

Then

$$\begin{aligned}\mathbf{S}^{(-)}(\mathbf{r})&=\overline{\mathbf{s}}_a(\mathbf{r})-\overline{\mathbf{s}}_b(\mathbf{r})\\&\sim(R_1^\dagger\boldsymbol{\sigma}L_1-R_2^\dagger\boldsymbol{\sigma}L_2)+\text{H.c.}\\&\sim\cos(\sqrt{\pi}\Phi_c^{(+)})\cos(\sqrt{\pi}\Phi_c^{(-)})\sigma_0\mathbf{N}\\&\quad-\sin(\sqrt{\pi}\Phi_c^{(+)})\sin(\sqrt{\pi}\Phi_c^{(-)})\mu_0\tilde{\mathbf{N}}.\end{aligned} \tag{24}$$

The OP $\mathbf{S}^{(-)}(\mathbf{r})$ is coherent in the Haldane spin-liquid phase *B*, the corresponding particle representing a massive triplet magnon. Note that in the expression (24) the vector field $\mathbf{N}$ plays the role of the staggered magnetization of the effective antiferromagnetic spin-1 chain.[8]

In full analogy with the BDW OP (19), one can construct the site-off-diagonal staggered magnetization

$$\begin{aligned}\boldsymbol{\Sigma}^{(-)}(\mathbf{r})&=\tfrac{1}{2}\psi_a^\dagger(\mathbf{r})\boldsymbol{\sigma}[\psi_b(\mathbf{r}+\mathbf{e}_1)-\psi_b(\mathbf{r}-\mathbf{e}_2)]\\&\quad-\tfrac{1}{2}[\psi_a^\dagger(\mathbf{r}+\mathbf{e}_1)-\psi_a^\dagger(\mathbf{r}-\mathbf{e}_2)]\sigma\psi_b(\mathbf{r})\\&\sim\frac{i}{2}(R_1^\dagger\boldsymbol{\sigma}L_1-R_2^\dagger\boldsymbol{\sigma}L_2)+\text{H.c.}\\&\sim\cos(\sqrt{\pi}\Phi_c^{(+)})\sin(\sqrt{\pi}\Phi_c^{(-)})\mu_0\mathbf{N}\\&\quad+\sin(\sqrt{\pi}\Phi_c^{(+)})\cos(\sqrt{\pi}\Phi_c^{(-)})\sigma_0\tilde{\mathbf{N}}.\end{aligned} \tag{25}$$

The structure of Eq. (25) indicates that phase *E* represents a Haldane spin liquid and is dual to phase *B*. Indeed, in phase *E* it is the vector field $\tilde{\mathbf{N}}$ that can be regarded as the staggered magnetization of the effective $S=1$ chain, and, hence, the spectral weight of the operator $\boldsymbol{\Sigma}^{(-)}$ contains in this phase a coherent triplet magnon.

Pairing operators. Let us construct the *s-wave superconducting (SC) order parameter* Δ_{sSC}. To this end, we first build locally averaged, site-diagonal, singlet pairing operators:

$$\begin{aligned}\Delta_{sSC}^\nu(\mathbf{r})&=\tfrac{1}{3}[\psi_{\nu,\uparrow}\psi_{\nu,\downarrow}(\mathbf{r})+\psi_{\nu,\uparrow}\psi_{\nu,\downarrow}(\mathbf{r}+\mathbf{e}_1)\\&\quad+\psi_{\nu,\uparrow}\psi_{\nu,\downarrow}(\mathbf{r}-\mathbf{e}_2)],\quad\nu=a,b.\end{aligned}$$

The OP Δ_{sSC} is then defined as

$$\begin{aligned}\Delta_{sSC}(\mathbf{r})&=\Delta_{sSC}^a(\mathbf{r})+\Delta_{sSC}^b(\mathbf{r})\\&\sim\sum_\sigma\sigma(L_{1\sigma}R_{2,-\sigma}-L_{2\sigma}R_{1,-\sigma})\\&\sim\kappa_{1\uparrow}\kappa_{2\downarrow}e^{-i\sqrt{\pi}\Theta_c^{(+)}}(\cos\sqrt{\pi}\Phi_c^{(-)}\sigma_1\sigma_2\sigma_3\mu_0\\&\quad+i\sin\sqrt{\pi}\Phi_c^{(-)}\mu_1\mu_2\mu_3\sigma_0).\end{aligned} \tag{26}$$

The amplitude of this OP acquires a finite value in non-Haldane phases *C* and *F*. These two phases, with coherent singlet magnetic modes in their spectrum at half filling, exhibit power-laws SC correlations under doping.

The *s*-wave-type superconductivity is not the only possible singlet SC order one can imagine. One can introduce *SC order* parameter which transforms nontrivially under the point group

$$\begin{aligned}\Delta_{mSC}&=\tfrac{1}{3}\psi_{a\uparrow}(\mathbf{r})[\psi_{b\downarrow}(\mathbf{r})-\psi_{b\downarrow}(\mathbf{r}+\mathbf{e}_1)\\&\quad-\psi_{b\downarrow}(\mathbf{r}-\mathbf{e}_2)]-(\uparrow\leftrightarrow\downarrow)\\&\sim\sum_\sigma\sigma(L_{1\sigma}R_{2,-\sigma}+L_{2\sigma}R_{1,-\sigma})+\text{oscillatory terms}\\&\sim e^{-i\sqrt{\pi}\Theta_c^{(+)}}[\cos(\sqrt{\pi}\Phi_c^{(-)})\mu_1\mu_2\mu_3\sigma_0\\&\quad+i\sin(\sqrt{\pi}\Phi_c^{(-)})\sigma_1\sigma_2\sigma_3\mu_0].\end{aligned} \tag{27}$$

This pairing OP exhibits power-law correlations in doped Haldane phases *B* and *E*.

To see what kind of superconductivity this is, let us consider the lattice mean-field Hamiltonian

$$\begin{aligned}H&=(\psi_{a\uparrow}^+,\psi_{b\downarrow}^+,\psi_{a\downarrow},\psi_{b\uparrow})\\&\times\begin{pmatrix}0&t(k)&0&g(k)\Delta\\t^*(k)&0&-g(k)\Delta&0\\0&-g^*(k)\Delta^*&0&t(k)\\g^*(k)\Delta^*&0&t^*(k)&0\end{pmatrix}\\&\times\begin{pmatrix}\psi_{a\uparrow}\\\psi_{b-\downarrow}\\\psi_{a\downarrow}^+\\\psi_{b-\uparrow}^+\end{pmatrix},\end{aligned} \tag{28}$$

where $g(k)=-1+2\cos(k_x/2)e^{i\sqrt{3}k_y/2}$. The spectrum is

$$E^2=|t(k)|^2+|g(k)|^2|\Delta|^2. \tag{29}$$

In the Haldane phase *C* under doping we get the following OP:

$$\psi_{a\sigma}\partial_x\psi_{b-\sigma}-\psi_{a-\sigma}\partial_x\psi_{b\sigma}. \tag{30}$$

The *Aharonov-Bohm* effect: the *y* component of the vector potential is coupled to

$$(R^+_{1\sigma}L_{1\sigma}+L^+_{1\sigma}R_{1\sigma})-(R^+_{2\sigma}L_{2\sigma}+L^+_{2\sigma}R_{2\sigma})$$
$$\sim\cos(\sqrt{\pi}\Phi_c^{(+)})\sin(\sqrt{\pi}\Phi_c^{(-)})\sigma_1\sigma_2\sigma_3\sigma_0$$
$$-\sin(\sqrt{\pi}\Phi_c^{(+)})\cos(\sqrt{\pi}\Phi_c^{(-)})\mu_1\mu_2\mu_3\mu_0. \quad (31)$$

It is coherent in Haldane phase E with an emission of the magnetic singlet.

The *staggered flux* around a hexagonal plaquette is

$$\Phi=6e^{i\pi/6}e^{2iQx}(L_2^+L_1-R_2^+R_1)+\text{H.c.}$$
$$\sim(R_f\chi_R^{(0)}-L_f\chi_L^{(0)})e^{2iQx+i\pi/6}+\text{H.c.}, \quad (32)$$

where the flavor fermion is associated with $\Phi_c^{(-)}$ field. Therefore there is an interesting possibility to drive a system into a peculiar critical state with a mixture of the magnetic singlet and nonmagnetic orbital mode by applying a magnetic field with the corresponding period.

V. SMALL DOPING

The large velocity difference between the symmetric charge modes and the other part of the spectrum holds a key to the stability of the approach at finite doping. For small doping $k_Fa\ll\exp(-\pi v/2e^2)$ the soliton mode of $\Phi_c^{(+)}$ field, though becoming gapless, still lies above the others in the most of the momentum space [see Fig. 2(b)]. This means that one can still integrate over $\Phi_c^{(+)}$ and obtain Eq. (9) though with a prefactor <1. Thus a small doping will decrease the gaps. It may also give rise to finite decay rates for the collective modes. This is a pseudogap regime which is perhaps similar to the one existing in the underdoped state of the cuprate superconductors (see, for example, the recent paper.[13] The physics of this regime will be governed by two energy scales: the scale of collective modes M_c [see Eq. (10)] and the electronic scale M_e. At energies smaller than M_c the system is a Luttinger liquid, at $M_c<E<M_e$ the collective modes contribute to all physical properties giving rise to strong enhancement of the magnetic susceptibility and specific heat. Above M_e the effects of backscattering disappear.

Let us briefly discuss a possible enhancement of the superconducting fluctuations in a doped regime. In those phases where the amplitude of the SC order parameter is frozen (see the discussion above) its power-law correlations are determined by the scaling dimension of operator $\exp[i\sqrt{\pi}\Theta_+^{(c)}]$. This scaling dimension is equal to $1/4\tilde{K}_c$ where $\tilde{K}_c$ is the renormalized Luttinger constant. At large doping the value of this constant is determined by the long-distant Coulomb interaction and is small, but close to the transition (small doping) it is close to one (see Ref. 14 for a more detailed analysis). Therefore there is a window of doping where $\tilde{K}_c<1/2$ where the pairing susceptibility diverges. A more detailed description of the pseudogap regime will be given elsewhere.

VI. CONCLUSION

Let us summarize our results. We have analyzed the effect of the long-range Coulomb interaction on the low-energy properties of the armchain nanotube. We have shown that the spectrum of the system is very rich. The phase diagram includes six phases differing from each other by their response functions. Under doping four of them have enhanced superconducting fluctuations.

SWCN's exhibit two types of behavior: either band insulators or Luttinger liquids. Armchair CN's are believed to be metallic and be of the Tomonaga-Luttinger (TLL) type. This, in fact, is only true away from 1/2 filling. As shown in this paper, the picture changes dramatically at 1/2 filling when effects of strong correlations become crucial. To observe these effects in experimental conditions, the chemical potential must be fine tuned to the value $\mu=0$ at which the Fermi ''surface'' is represented by two degeneracy (Dirac) points. Then, due to the special role of Umklapp processes in the presence of unscreen Coulomb interaction, on lowering the temperature, one must be able to see a crossover from the metallic, TLL behavior to an insulator discussed in the paper. Such insulating state is Mott-type, with a much richer spectrum than in the Hubbard model. One important difference is that, unlike in the Hubbard model, the spin excitations have spectral gaps.

The estimates of interaction matrix elements for carbon nanotubes are provided in[3]:

$$g_i=\beta_i\frac{e^2}{N\epsilon}, \quad i=c,t,s$$

$$\beta_c\approx0.4, \quad \beta_t\approx0.5, \quad \beta_s\approx-1.3, \quad (33)$$

where N is the number of transverse bands of the nanotube and $\epsilon\approx1.4$ is the dielectric constant. These estimates indicate that realistic nanotubes belong to phase B. Equation (10) also gives the following estimates for the spectral gaps of the collective modes:

$$|M_i|=|\beta_i|\frac{e^2}{\pi N\alpha\epsilon}\frac{v}{v_c}. \quad (34)$$

Since α is the short distance cutoff of the bosonic theory and is therefore non universal, this formula contains a certain degree of ambiguity. For noninteracting electrons $\pi\alpha=a_0$ (the lattice spacing). Taking $N=10$, $v/v_c=1/3$, and $a_0=0.246$ nm we get the estimate of order of 0.1 eV. The single-particle gaps should be even greater.

Since the gaps should be quite sizable, one may wonder whether they have not been already observed. The existing techniques produce simultaneously carbon nanotubes of different sizes and chiralities and one has to select the relevant ones using some criteria. The simplest one is to differ between metallic and insulating (semiconductor) nanotubes. Naturally, on the first glance Mott and band insulators look alike. Therefore it is possible that the Mott insulating armchair nanotubes have been overlooked being taken for semiconducting ones. To distinguish Mott insulator from a band one has to measure transport and magnetic properties and

compare the gaps. The clearest sign of 'mottness' is the difference in gap sizes in different response functions. This is the feature to look for experimentally.

ACKNOWLEDGMENTS

We are grateful to P. Azaria, A. O. Gogolin, Ph. Lecheminant, A. Chubukov, P. Coleman, and F. H. L. Essler for fruitful discussions. A.M.T. acknowledges support from U.S. Department of Energy under Contract No. DE-AC02-98CH10886 and a kind hospitality of Abdus Salam ICTP where a part of the work was conducted. A.A.N. was partly supported by MIUR, under Project COFIN2003 ''Field Theory, Statistical Mechanics, and Electron Systems.'' He also acknowledges the support from the Institute for Theory of Strongly Correlated and Complex Systems at Brookhaven.

APPENDIX A

The original Hamiltonian describing noninteracting electrons on a honeycomb lattice can be compactly written in the two-sublattice (Nambu) representation

$$H_0=\sum_{\mathbf{k}} \Psi_{\mathbf{k}}^{\dagger}\mathcal{H}(\mathbf{k})\Psi_{\mathbf{k}}, \tag{A1}$$

where

$$\Psi_{\mathbf{k}}=\begin{pmatrix}\psi_a(\mathbf{k})\\ \psi_b(\mathbf{k})\end{pmatrix}, \quad \mathcal{H}(\mathbf{k})=\begin{pmatrix}0 & t(\mathbf{k})\\ t^*(\mathbf{k}) & 0\end{pmatrix}, \tag{A2}$$

$$t(\mathbf{k})=1+2\cos(k_x/2)e^{i(\sqrt{3}/2)k_y}, \tag{A3}$$

and the sum in Eq. (A1) goes over the Brillouin zone. The spectrum has two degeneracy points (nodes) at $\mathbf{Q}_{1,2}=(\pm 4\pi/3,0)$. Linearizing the noninteracting Hamiltonian near these points yields two cones associated with $(2+1)$-dimensional massless Dirac fermions:

$$\mathcal{H}(\mathbf{Q}_{1,2}+\mathbf{p})=v(\tau_y p_y \mp \tau_x p_x), \quad v=\sqrt{3}t/2. \tag{A4}$$

When a two-dimensional sheet of graphite is wrapped to produce an armchair nanotube, k_y gets quantized, and the lowest-energy subband corresponding to $k_y=0$ stays gapless. The resulting problem is one dimensional because the wave function does not depend on y. Projecting the fermionic annihilation operators of the a and b sublattices onto the $k_y=0$ subspace, we get

$$\begin{pmatrix}\psi_a(\mathbf{r})\\ \psi_b(\mathbf{r})\end{pmatrix}\to e^{iQx}\begin{pmatrix}r_1(x)\\ l_1(x)\end{pmatrix}+e^{-iQx}\begin{pmatrix}r_2(x)\\ l_2(x)\end{pmatrix}. \tag{A5}$$

The effective 1D Hamiltonian is brought to its canonical diagonal form

$$H_0=-iv\sum_{j=1,2}\int dx \;\; (R_j^{\dagger}\partial_x R_j - L_j^{\dagger}\partial_x L_j) \tag{A6}$$

by linear transformations

$$r_1=(R_1+L_1)/\sqrt{2}, \quad l_1=(-R_1+L_1)/\sqrt{2},$$

$$r_2=(R_2-L_2)/\sqrt{2}, \quad l_2=(R_2+L_2)/\sqrt{2}. \tag{A7}$$

The structure of these transformations reflects the fact that different Dirac points, $k_x=Q$ and $k_x=-Q$, are not associated with fermions of different chiralities, as it is the case for standard chains and ladders; instead each of these points is characterized by a pair of right (R_j) and left (L_j) fields. This is because the gapless spectrum of the armchair nanotube keeps the memory of the two-cone Dirac structure of the dispersion law in the 2D graphite (in fact, the 1D spectrum is obtained from the 2D one by cutting the two cones by the plane $k_y=0$). For this reason, in case of nanotubes, smooth components of the physical fields are contributed not only by the diagonal ''currents,'' $R_j^{\dagger}R_j$, and $L_j^{\dagger}L_j$, but also by off-diagonal ''mass bilinears,'' $R_j^{\dagger}L_j$, and $L_j^{\dagger}R_j$.

The chiral fermionic fields can be bosonized in terms of chiral bosonic fields $\Phi_{j\sigma}^{R,L}$,

$$\begin{pmatrix}R_{j\sigma}\\ L_{j\sigma}\end{pmatrix}=\frac{\kappa_{j\sigma}}{\sqrt{2\pi\alpha}}e^{\pm i\sqrt{4\pi}\Phi_{j\sigma}^{R,L}}, \quad j=1,2, \quad \sigma=\pm 1,$$

$$[\Phi_{j\sigma}^{R},\Phi_{j',\sigma'}^{L}]=\frac{i}{4}\delta_{jj'}\delta_{\sigma\sigma'}. \tag{A8}$$

Here α is the short-distance cutoff in the bosonic theory, and $\kappa_{j\sigma}$ are Klein factors obeying the algebra $\{\kappa_{j\sigma},\kappa_{j'\sigma'}\}=\delta_{jj'}\delta_{\sigma\sigma'}$. The product of the four Klein factors $\Gamma=\kappa_{1\uparrow}\kappa_{1\downarrow}\kappa_{2\uparrow}\kappa_{2\downarrow}$ satisfies $\Gamma^2=1$. Since Γ is not a dynamical variable, we can conveniently choose $\Gamma=1$.

In the bulk of this paper, we adopted the description in terms of four scalar fields $\Phi_c^{(\pm)}$, $\Phi_s^{(\pm)}$ and their dual counterparts $\Theta_c^{(\pm)}$, $\Theta_s^{(\pm)}$, known from earlier studies of the two-channel Kondo problem.[15] These fields describe the symmetric and antisymmetric charge excitations (equivalently, the ''charge'' and flavor modes),

$$\Phi_c^{(\pm)}=\tfrac{1}{2}(\Phi_{1\uparrow}+\Phi_{1\downarrow}\pm\Phi_{2\uparrow}\pm\Phi_{2\downarrow}), \tag{A9}$$

as well as the symmetric and antisymmetric spin excitations (or the ''spin'' and ''spin-flavor'' modes),

$$\Phi_s^{(\pm)}=\tfrac{1}{2}(\Phi_{1\uparrow}-\Phi_{1\downarrow}\pm\Phi_{2\uparrow}\mp\Phi_{2\downarrow}). \tag{A10}$$

Here $\Phi_{j\sigma}=\Phi_{j\sigma}^{R}+\Phi_{j\sigma}^{L}$. The corresponding dual fields $\Theta_c^{(\pm)}$ and $\Theta_s^{(\pm)}$ are obtained from the above expressions by replacing $\Phi_{j\sigma}$ by $\Theta_{j\sigma}=-\Phi_{j\sigma}^{R}+\Phi_{j\sigma}^{L}$.

APPENDIX B

The interaction can be written as

$$[\rho_a+\rho_b](\mathbf{r}_1)V_{aa}(\mathbf{r}_{12})[\rho_a+\rho_b](\mathbf{r}_2) + 2\rho_a(\mathbf{r}_1)[V_{ab}(\mathbf{r}_{12})-V_{aa}(\mathbf{r}_{12})]\rho_b(\mathbf{r}_2), \tag{B1}$$

where, in the low-energy limit, the local electron densities on the a and b sublattices are represented by

$$\rho_a(\mathbf{r})\to\rho_r(x)+e^{2iQx}M_r(x)+e^{-2iQx}M_r^{+}(x),$$

$$\rho_b(\mathbf{r})\to\rho_l(x)+e^{2iQx}M_l(x)+e^{-2iQx}M_l^{+}(x),$$

$$\rho_r = r_1^+ r_1 + r_2^+ r_2, \quad \rho_l = l_1^+ l_1 + l_2^+ l_2,$$

$$M_r = r_2^+ r_1, \quad M_l = l_2^+ l_1. \tag{B2}$$

Substituting Eq. (B2) into Eq. (B1) and dropping the oscillatory terms we get four terms:

$$(\rho_r + \rho_l)_1 V_{aa}(\mathbf{r}_{12})(\rho_r + \rho_l)_2,$$

$$2[U_{ab}(0) - U_{aa}(0)]\rho_r(x)\rho_l(x),$$

$$2U_{aa}(2Q)[M_r(x)M_r^+(x) + M_l(x)M_l^+(x)],$$

$$2U_{ab}(2Q)(M_r M_l^+ + M_l M_r^+),$$

where $U(0)$ and $U(2Q)$ stand for the Fourier transforms of the interaction potentials. The first term here gives the Luttinger coefficient renormalization. The ''backscattering'' interaction expressed in terms of the standard Dirac fermions with flavor indices 1,2 looks as follows:

$$\begin{aligned} &\tfrac{1}{2} g_1 (R_{1,\sigma}^+ L_{1,\sigma} - R_{2,\sigma}^+ L_{2,\sigma} + \text{H.c.})^2 \\ &\quad + g_2[(L_{2,\sigma}^+ L_{1,\sigma})(R_{1,\sigma'}^+ R_{2,\sigma'}) + \text{H.c.}] \\ &\quad + g_3 (L_{2,\sigma}^+ R_{1,\sigma} - R_{2,\sigma}^+ L_{1,\sigma})(L_{1,\sigma'}^+ R_{2,\sigma'} - R_{1,\sigma'}^+ L_{2,\sigma'}), \end{aligned} \tag{B3}$$

where the couplings are expressed in terms of the Fourier components of the interaction:

$$g_1 = U_{aa}(0) - U_{ab}(0),$$

$$g_2 = U_{ab}(2Q) - U_{aa}(2Q), \quad g_3 = U_{aa}(2Q) + U_{ab}(2Q). \tag{B4}$$

In the UV model, which apart from the Hubbard (on-site) interaction U also includes the interaction between electrons on nearest-neighbor sites V, the couplings g_i are given by

$$g_1 = U - 3V, \quad g_2 = -U, \quad g_3 = U. \tag{B5}$$

The bare Hamiltonian for R,L is standard

$$H_0 = iv \int dx [L_a^+ \partial_x L_a - R_a^+ \partial_x R_a]. \tag{B6}$$

As already explained in Secs. I and II, in the presence of long-range Coulomb potential, Umklapp processes with the structure $R_1^\dagger R_2^\dagger L_3 L_4 + \text{H.c.}$ represent the strongly relevant part of interaction (B3). In the bosonic language, these are the processes containing the symmetric charge field Φ_c^+. Using bosonization rules (A8)–(A10), one straightforwardly derives Eq. (6). The g_2 part of (B3) does not contribute.

[1] R. Egger and A.O. Gogolin, Phys. Rev. Lett. **79**, 5082 (1997).
[2] C. Kane, L. Balentz, and M.P.A. Fisher, Phys. Rev. Lett. **79**, 5086 (1997).
[3] H. Yoshioka and A.A. Odintsov, Phys. Rev. Lett. **82**, 374 (1999); Phys. Rev. B **59**, R10 457 (1999).
[4] L. Levitov and A.M. Tsvelik, Phys. Rev. Lett. **90**, 016401 (2003).
[5] L. Glazman *et al.*, Phys. Rev. B **45**, 8454 (1992); H.J. Schulz, Phys. Rev. Lett. **71**, 1864 (1993).
[6] R. Saito, G. Dresselhaus, and M. S. Dresselhaus, *Physical Properties of Carbon Nanotubes* (Imperial College Press, London, 1998).
[7] C. Wu, W.V. Liu, and E. Fradkin, Phys. Rev. B **68**, 115104 (2003).
[8] D. Shelton, A.A. Nersesyan, and A.M. Tsvelik, Phys. Rev. B **53**, 8521 (1996); A. O. Gogolin, A. A. Nersesyan, and A. M. Tsvelik, *Bosonization in Strongly Correlated Systems* (Cambridge University Press, Cambridge, 1999).
[9] D.G. Shelton and A.M. Tsvelik, Phys. Rev. B **53**, 14 036 (1996).
[10] I.V. Krive, A.A. Nersesyan, M. Jonson, and R.I. Shekhter, Phys. Rev. B **52**, 10 865 (1995).
[11] H.H. Lin, L. Balentz, and M.P.A. Fisher, Phys. Rev. B **58**, 1794 (1998).
[12] Al.B. Zamolodchikov, Int. J. Mod. Phys. A **10**, 1125 (1995).
[13] U. Schollwöck, S. Chakravarty, J.O. Fjaerestad, J.B. Marston, and M. Troyer, Phys. Rev. Lett. **90**, 186401 (2003).
[14] E. Papa and A.M. Tsvelik, Phys. Rev. B **63**, 5109 (2001).
[15] V.J. Emery and S. Kivelson, Phys. Rev. B **47**, 10 812 (1992).